



How relevant are frequency changes of weather regimes for understanding climate change signals in surface precipitation in the North Atlantic–European sector? A conceptual analysis with CESM1 large ensemble simulations

Luise J. Fischer^{1,2,a}, David N. Bresch^{2,3}, Dominik Büeler^{4,1,3}, Christian M. Grams^{4,3}, Robin Noyelle¹, Matthias Röthlisberger¹, and Heini Wernli¹

¹Institute for Atmospheric and Climate Science, ETH Zürich, Zurich, Switzerland

²Institute for Environmental Decisions, ETH Zürich, Zurich, Switzerland

³Federal Office of Meteorology and Climatology, MeteoSwiss, Zurich, Switzerland

⁴Institute of Meteorology and Climate Research (IMK-TRO), Department Troposphere Research, Karlsruhe Institute of Technology (KIT), Karlsruhe, Germany

^apresent address: South Pole, Melbourne, Australia

Correspondence: Heini Wernli (heini.wernli@env.ethz.ch)

Received: 26 April 2024 – Discussion started: 16 May 2024

Revised: 24 June 2025 – Accepted: 11 July 2025 – Published: 29 September 2025

Abstract. Climate change affects the climatology of surface precipitation in spatially inhomogeneous ways, and it is challenging to identify and quantify the contribution of atmospheric circulation changes to this pattern. Various methods have been developed to characterize the large-scale atmospheric circulation and assess its changes, e.g., by classifying the flow into so-called weather regimes or circulation types. Several studies have then related frequency changes of these regimes due to global warming to changes in surface weather parameters. However, even without regime frequency changes, the climatology of surface parameters may change due to so-called regime intensity changes (e.g., a particular regime becomes on average wetter or drier). In this study, the question of how relevant frequency changes of weather regimes are for understanding climate change signals in surface precipitation is addressed with a novel conceptual framework. For every regime i , a spatially varying parameter $\gamma_i(P)$ is introduced, which corresponds to the ratio of the contributions from regime frequency vs. regime intensity changes to the climate change signal of precipitation P . Conceptual considerations show that $\gamma_i(P)$ is (i) proportional to the relative change of regime frequency, (ii) proportional to the regime-specific anomaly of precipitation, and (iii) inversely proportional to the climate change effect on

regime intensity. The combination of these independent and competing factors makes the study of $\gamma_i(P)$ interesting and insightful. As a specific example application of this framework, we consider a 7-category weather regime classification in the North Atlantic–European sector and large ensemble simulations with the CESM1 climate model under the RCP8.5 emission scenario for the periods 1990–1999 and 2091–2100. Considering $\gamma_i(P)$ for surface precipitation, P in this simulation setup reveals that (1) γ values are typically less than 0.25 and therefore, to first order, frequency changes of weather regimes (WRs) are of secondary importance for explaining climate change signals in P – in contrast, the intensity changes dominate, which are to a large degree, but not entirely, related to the so-called thermodynamic effects of global warming; (2) the main reason for the generally low values of γ is the comparatively small WR frequency changes and the limited regime-specific anomalies of P , in particular over continental Europe; and (3) γ values tend to be slightly larger for precipitation variables that are less constrained by thermodynamic arguments, i.e., γ for the number of wet days is larger than γ for the number of heavy-precipitation days. In summary, this study provides a generally applicable framework to quantify climate change effects of regime frequency changes on surface parameters, it illus-

trates the key conditions that must be fulfilled such that these frequency changes can become relevant, and, at least in our application, it shows that these conditions are generally not fulfilled.

1 Introduction

Given the complex, chaotic nature of the large-scale atmospheric flow with the repeated occurrence of similar flow patterns, over many decades meteorologists and climatologists have attempted to sort the daily flow patterns into distinct categories. Early examples are the so-called “Grosswetterlagen” by Hess and Brezowsky (1952) with 30 types for Europe and the weather types by Schüepp (1959) for the European Alps with 6 classes and 33 types (Bader and Richner, 2018). Namias (1968) discussed the role of “weather typing” for extended and long-range forecasts of daily precipitation in the US and the history of these ideas that go back to the late 19th century. These early classifications were, like any classification of atmospheric flows, based on specific choices of the region of interest, the variables and vertical levels to be considered, and the number of categories to be determined.

While these early classification schemes relied on mainly subjective criteria, more objective methods, for instance based on principal component analysis (sometimes combined with clustering analysis), have been developed in the last decades (e.g., Barnston and Livezey, 1987) and have led to many flow classifications. Different names have been used for the flow categories, e.g., circulation types/regimes or weather types/regimes. The COST Action 733 compared 71 such circulation type classifications for central Europe, which illustrates the multitude of existing approaches (Tveito and Huth, 2016). An important example is the classification by Vautard (1990) with four weather regimes (WRs) identified for the North Atlantic–European region in winter, based on low-pass-filtered geopotential height at 700 hPa (i.e., with the transient synoptic variability filtered out). This classification has been extended recently by Grams et al. (2017), who identified seven WRs in all seasons based on low-pass-filtered geopotential height at 500 hPa in a similarly large domain. Addressing the fundamental question of whether WRs represent physical modes of the atmosphere or are merely useful statistical categorizations, Hochman et al. (2021) used concepts from dynamical systems theory and found evidence that most WRs identified by Grams et al. (2017) are physically meaningful and suitable for addressing circulation responses in a changing climate. For a broader discussion about the usefulness of circulation regimes, the interested reader is referred to the review by Hannachi et al. (2017).

One of the key properties of these classic WRs is that they characteristically link the lower-frequency and thus more predictable evolution of the large-scale circulation to regional surface weather. They have thus become a popular

tool in weather and climate science in recent years. In the context of today’s climate, WRs are used to understand and classify the variability in regional surface weather and related socio-economic parameters in various regions around the world. For instance, they have been shown to modulate, in certain regions, the occurrence of extreme temperature, extreme precipitation, or surface wind speed (Yiou and Nogaj, 2004; Pasquier et al., 2019; Mastrantonas et al., 2020; Coe et al., 2021; Zhang and Wang, 2021; Madonna et al., 2021); renewable energy production (Jerez and Trigo, 2013; Grams et al., 2017; van der Wiel et al., 2019; Drücke et al., 2021); aerosol transport and concentration (Gaetani et al., 2021); air pollution (Maddison et al., 2021); or human excess mortality (Huang et al., 2020). WRs are thus increasingly identified in operational weather forecasts – particularly on subseasonal-to-seasonal lead times, by which predictability arises from slowly varying planetary-scale phenomena that modulate WR variability on multi-day to weekly timescales (Palmer, 1999; Lang et al., 2020). Categorical WR forecasts as predictors for regional surface weather can thus be beneficial at these lead times compared to direct model output of surface weather variables on a grid-point level (Vigaud et al., 2018; Bloomfield et al., 2021).

In the context of past and future climates, WRs are often used to understand the relative contributions of changes in large-scale variability (i.e., in WR occurrence) and of thermodynamic changes to surface weather changes between different climate conditions. For instance, Yiou et al. (2012) showed that pattern or frequency changes of the four main North Atlantic–European WRs are too small to explain the substantial temperature changes Europe experienced between the Medieval Warm Period (10th–13th centuries) and the Little Ice Age (16th–19th centuries). Likewise, Horton et al. (2015) argued that more recent trends in Northern Hemisphere extreme surface temperature were primarily driven by thermodynamic changes, although changes in WR frequency and duration were important for specific regions. Nevertheless, distinguishing between thermodynamic and dynamic climate change effects not only improves our physical understanding, but also helps in assessing how robust the projected regional surface weather changes might be based on their contributing processes. For instance, future changes in the frequency and intensity of Northern Hemisphere cold extremes in winter will result from a complex superposition of changes in global mean temperature, in cold-air outbreak intensity due to Arctic amplification, in the frequency of stratospheric polar vortex disruptions due to changes in stratospheric dynamics, and in midlatitude Rossby wave activity due to changes in baroclinicity. The last of these processes is directly related to WR occurrence. However, there is rather low consensus on future changes in WR occurrence and their role in surface weather changes. For instance, for the positive and negative phases of the North Atlantic Oscillation (NAO), which are considered distinct WRs in several North Atlantic/European WR

classifications, Cattiaux et al. (2013) found an increasing frequency of the negative NAO phase in CMIP5 projections, while Fabiano et al. (2021) detected an increasing frequency of the positive NAO phase in CMIP6 projections. Huguenin et al. (2020), considering a WR classification over central Europe, found that most WR frequency changes towards the end of the 21st century are small and not consistent across different climate models. The relative contribution of these future WR frequency changes to surface weather changes has also been shown to differ, depending on the region, season, and surface parameter. While Riediger and Gratzki (2014) and Santos et al. (2016) found, alongside a likely thermodynamic background signal, a relatively important contribution of future WR changes to changes in surface temperature and precipitation in western and central Europe, Cattiaux et al. (2013) attributed a rather minor role to these changes.

This study aims at contributing to this research theme, which connects climate change, WRs, and surface weather, by introducing a conceptual framework that provides insight into why, where, and when WR frequency changes can matter for understanding climate change effects on surface weather. The conceptual framework will be illustrated with a particular choice of WRs in the North Atlantic–European region, climate simulations, and surface weather parameters. Importantly, we do not attempt to provide a “final answer” regarding the role and relevance of WR frequency changes for understanding climate change signals, but rather we develop a framework that allows the quantitative analysis of the factors that determine this role. To be more specific, the main objectives of this study are to

1. provide a conceptual view on the conditions that determine whether WR frequency changes are relevant to explaining climate change signals of a specific parameter ϕ , in comparison to intensity changes (to quantitatively assess this relevance, we will introduce a field $\gamma_i(\phi)$, which can be calculated for any choice of WR classification with regimes $i = 1, \dots, n$ and parameter ϕ), and
2. quantify $\gamma_i(\phi)$, for mean precipitation $\phi = P$, the number of wet days $\phi = N_{\text{wet}}$ and the number of heavy-precipitation days $\phi = N_{\text{heavy}}$, based on large ensemble climate simulations and a specific WR classification.

We first introduce, in Sect. 2, the climate simulation data sets and the WR classification used in this study and then, in Sect. 3, the field $\gamma_i(\phi)$, which serves to address the above objective 1. Example applications of this concept to climate change signals in surface precipitation are presented in Sect. 4 (objective 2), and in Sect. 5 the main conclusions are summarized and critically discussed.

2 Climate simulations and WR identification

This study uses global large ensemble climate simulations for a historical and future period under the RCP8.5 emission

scenario (Sect. 2.1), and a 7-category all-season WR classification for the North Atlantic–European region is applied to output from these simulations (Sect. 2.2 and 2.3).

2.1 CESM1-LE climate simulations

The coupled ocean–atmosphere climate simulations used in this study were performed with version 1 of the Community Earth System Model (CESM1) (Hurrell et al., 2013). Six-hourly fields of geopotential height at 500 hPa, Z_{500} , and surface precipitation P , on a regular grid with a horizontal resolution of approximately 1° , were obtained through re-runs of the CESM1-LE simulations (Kay et al., 2015), which are described in more detail in R  thlisberger et al. (2020). In this study, data from simulations with external forcing from two specific decades are investigated separately, one period covering the years 1990–1999 and the second one covering the years 2091–2100, henceforth referred to as historical and future (or end-of-century) simulations, respectively. For both periods, the data sets consist of 35 ensemble members, each 10 years long, yielding 350 years with historical and future climate conditions, respectively. Note that due to the coupled nature of these simulations, the individual members only share the same external forcing and are independent in terms of their evolution of sea surface temperatures and the phases of, for instance, the El Ni  o–Southern Oscillation. Therefore, the 350 years in each climate period yields a very large sample of possible atmospheric responses to the external forcing that is specific for the respective decade. As this study will focus on the climate change effects on seasonal-mean P , model output was accumulated over the standard seasons of December–February (DJF), March–May (MAM), June–August (JJA), and September–November (SON), and values of P are given in units of mm d^{-1} . In addition to P , we will also consider the seasonal frequency of wet days N_{wet} (defined with a threshold of 1 mm d^{-1}) and of heavy-precipitation days N_{heavy} (defined with a threshold of the 99th percentile of daily precipitation values in the respective season in the historical simulations), and values of N_{wet} and N_{heavy} range between 0–1.

2.2 Year-round North Atlantic–European WRs

The 7-category all-season North Atlantic–European WR definition by Grams et al. (2017) is used in this study. The main reason for this specific choice is that this classification can be applied to all days of the year, providing a year-round categorization of the large-scale flow pattern in the North Atlantic–European sector. Grams et al. (2017) identified the WRs in the region extending from 80°W to 40°E and 30 to 90°N . They are based on an empirical orthogonal function (EOF) analysis of 6-hourly low-pass-filtered anomaly fields of Z_{500} , taken from ERA-Interim reanalysis data (Dee et al., 2011) from 1979 to 2015 and subsequent k -means clustering in the EOF space yielding the 7 WRs (i.e., 7 clusters). Further

details about this WR classification and how it can be applied to data from model simulations can be found in Grams et al. (2017) and Büeler et al. (2021), respectively.

The names of the WRs are based on the main flow pattern they represent and are as follows: Zonal Regime (ZO), Atlantic Trough (AT), Atlantic Ridge (AR), Scandinavian Trough (ScTr), Greenland Blocking (GL), European Blocking (EuBL), and Scandinavian Blocking (ScBL). The seven WRs explicitly capture different flavors of (strong) zonal flows and the occurrence of atmospheric blocking over Greenland, central Europe, and Scandinavia, respectively. If a Z_{500} anomaly field does not meet the classification criteria for any of the seven WR patterns, it is classified into a “no-regime category” (no). The interested reader can find illustrations of the average sea level pressure field and near-surface wind speed anomalies over Europe associated with these WRs in Grams et al. (2017, their Fig. 2). The no-regime category is very close to the overall climatology. For the time period 1979–2015, Grams et al. (2017) reported averaged annual WR frequencies of 31.5 % for the no-regime category and between 9.0 % (AT) and 10.9 % (ScBL) for the seven main WRs.

2.3 Identification of WRs in CESM1-LE

The WR classification introduced in Sect. 2.2 was applied to output from CESM1-LE, for both the historical and future periods. Importantly, when attributing a daily Z_{500} anomaly field from CESM1-LE to one of the WRs, we used the original ERA-Interim-based cluster mean Z_{500} patterns of the WRs identified by Grams et al. (2017); i.e., no separate EOF analysis was performed with fields from CESM1-LE. This pragmatic approach has the advantage that WR patterns remain unaltered and climate change can only modify the frequency of these patterns (this is further justified by theoretical argumentation that climate change will primarily change the frequency rather than the structure of quasi-stationary regimes; see Palmer, 1999). If separate EOF analyses were performed for the two climate simulation periods, then WRs would change both their pattern and their frequency, making the interpretation of the results from the decomposition approach (Sect. 3) less straightforward.

In this paragraph we provide additional technical information about how the WR classification, originally developed for reanalysis data, was applied to climate model data. For more details, the reader is referred to Sect. 4.2.4 in Fischer (2021) and Sect. 2.2 in Büeler et al. (2021). The key step is the projection of a simulated daily Z_{500} anomaly field onto the seven Z_{500} patterns of the ERA-Interim WRs, which in essence corresponds to the spatial correlation of the two fields. The anomalies of Z_{500} are computed relative to the climatology in the respective climate period. Following the approach by Michel and Rivi  re (2011), we then computed, for each daily Z_{500} anomaly and for each regime $i = 1, \dots, 7$, a non-dimensional regime index I_i . This index corresponds

to normalized anomalies of the projection for each regime i relative to the mean projection in the respective climate period, and the normalization is done with the climatological standard deviation of the projection in the respective climate period. Eventually, to determine the active weather regime at a given time, a set of so-called life-cycle criteria are applied to the time series of the regime indices. A regime i is considered “active” if its $I_i(t)$ is maximum among all seven indices at time t and equal to or above a threshold value of 0.98 for at least 5 consecutive days. This threshold value differs very slightly from the value of 1.0 used by Grams et al. (2017) in their ERA-Interim study. We decided to modify the threshold value such that we obtain the same percentage of no-regime days in the CESM1-LE historical simulation as we find in ERA-Interim for the years 1990–1999 (30.8 % averaged over all seasons). The fact that with such a soft tuning, we could obtain the same projection rate for any of the 7 regimes (almost 70 %) in CESM1-LE as in ERA-Interim serves as qualitative confirmation that the North Atlantic–European flow variability in the historical simulations compares favorably with reanalyses. For identifying WRs in the future climate simulations, the same procedure and the same threshold value of 0.98 are applied, leading to a slight reduction in the no-regime frequency (30.0 %).

Figure 1 shows the WR frequencies in DJF and JJA in the historical and future climate simulations. Note that these values differ from the ones reported in Fischer (2021, their Table B.2), as those were found to be affected by a programming error. In DJF, the regimes AT, ZO, and ScTr are more frequent (about 11 %–14 %) than the “blocked regimes” EuBL, ScBL, and GL (about 6 %–9 %), whereas the opposite is true in JJA (3 %–8 % vs. 11 %–17 %). These seasonal differences are consistent with the reanalysis-based results in Grams et al. (2017). Note that we expect some quantitative differences in $f_{\text{hist},i}$ in CESM1 compared to ERA-Interim, as CESM1 data for the historical period are only representative of the external forcing in the 1990s but not necessarily for the modes of decadal variability in this period; see discussion in Sect. 2.1. Most of the WR frequency changes from historical to future climate conditions ($\Delta f_i = f_{\text{ec},i} - f_{\text{hist},i}$) are modest. Relatively large values of Δf_i occur in DJF for the regimes AT (+1.3 %, corresponding to a relative increase of 9.4 %) and AR (−1.0 %, corresponding to a relative decrease of 10.1 %) and in JJA for the no-regime category (−3.7 %, corresponding to a relative decrease of 11.2 %) and in particular for the regime AR (+1.7 %, corresponding to a relative increase of 23.3 %).

3 Quantifying WR contributions to climate change signals

In this section, as the key methodological novelty of this study, we introduce a conceptual framework that serves to quantify the relevance of climate change effects on WR fre-

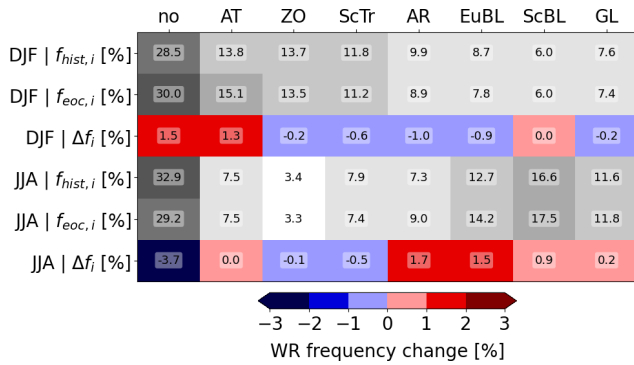


Figure 1. WR frequencies (in %) in DJF and JJA, respectively, in the CESM1 historical and future simulations ($f_{hist,i}$ and $f_{eoc,i}$), computed with 6 h Z_{500} fields. Also listed are the values of the climate change effect on WR frequencies, Δf_i . The frequency changes are statistically significant ($p < 0.001$) according to a χ^2 contingency test.

quencies to understanding climate change signals in a surface weather variable ϕ , such as precipitation. The starting point is to decompose this signal into contributions from changes related to WR frequency, Δf_i , and from changes related to what we call WR intensity, $\Delta \phi_i$, for instance the change in precipitation during WR i . This idea is written out explicitly in the following equations.

Let ϕ_p be the climatological value of the variable of interest (e.g., seasonal-mean precipitation) in period $p \in \{\text{hist}, \text{eoc}\}$ and $\phi_{p,i}$ be the climatological mean value of ϕ at all time steps in WR i in period p . The climate change signal on ϕ , i.e., the difference $\Delta \phi = \phi_{eoc} - \phi_{hist}$, can then be written as

$$\Delta \phi = \sum_{i=1}^n (f_{eoc,i} \phi_{eoc,i} - f_{hist,i} \phi_{hist,i}), \quad (1)$$

where $f_{p,i}$ is the frequency of WR i in period p and the summation is over all n WRs of a certain WR classification. Introducing the notation $\Delta \phi_i = \phi_{eoc,i} - \phi_{hist,i}$ and $\Delta f_i = f_{eoc,i} - f_{hist,i}$ to denote the climate change effect on the WR-specific intensity ϕ_i and on the frequency of WR i , respectively, Eq. (1) can be re-written as

$$\Delta \phi = \sum_{i=1}^n [(f_{hist,i} + \Delta f_i)(\phi_{hist,i} + \Delta \phi_i) - f_{hist,i} \phi_{hist,i}] \quad (2a)$$

$$= \sum_{i=1}^n \left[\underbrace{f_{hist,i} \Delta \phi_i}_{(i)} + \underbrace{\Delta f_i \phi_{hist,i}}_{(ii)} + \underbrace{\Delta f_i \Delta \phi_i}_{(iii)} \right]. \quad (2b)$$

Considering for instance precipitation, the three terms in Eq. (2b) then represent (i) the “contribution from the WR-specific precipitation intensity change to the climate change signal in precipitation”, (ii) the “contribution from WR frequency change to the climate change signal in precipitation”,

and (iii) a “residual” term due to concurrent changes in WR-specific precipitation intensity and WR frequency. It is important to mention that such decompositions were used in several previous studies and most likely the first time by Cassano et al. (2007), who quantified the role of frequency changes of synoptic flow patterns for global-warming-related changes in precipitation. Similar decompositions using circulation patterns or WRs were applied, for instance, by Horton et al. (2015) to temperature trends and by Cattiaux et al. (2013) to biases in climate models. And last but not least, this climate change partitioning method can also be applied to a specific weather system (e.g., extratropical cyclones) using a binary classification of days influenced by the weather system or not (Zappa et al., 2015). Several of the previous studies used the terminology introduced by Cassano et al. (2007) and referred to terms (i) and (ii) as the thermodynamic and dynamic (or circulation) change components, respectively.

Here, we further decompose term (ii), by considering the deviation of the mean WR-specific pattern from the climatology: $\phi_{hist,i}^* = \phi_{hist,i} - \phi_{hist}$; thus $\phi_{hist,i}^*$ is the WR-specific anomaly. Note that $\sum_{i=1}^n \phi_{hist,i}^* = 0$ by design. The interpretation of, e.g., a positive value of $\phi_{hist,i}^*$ is that during an active WR i , the variable ϕ is on average larger than in the climatology. Clearly, a WR-based analysis of a variable ϕ is particularly insightful if the values of $\phi_{hist,i}^*$ differ significantly from zero, at least for some WRs (i).

The second term on the right-hand side of Eq. (2b) can thus be written as

$$\Delta f_i \phi_{hist,i} = \Delta f_i (\phi_{hist} + \phi_{hist,i}^*) \quad (3a)$$

$$= \Delta f_i \phi_{hist} + \Delta f_i \phi_{hist,i}^*. \quad (3b)$$

Inserting this into Eq. (2b), the decomposition of the climate change signal on ϕ reads

$$\phi_{eoc} - \phi_{hist} = \sum_{i=1}^n \left[\underbrace{f_{hist,i} \Delta \phi_i}_{(i)} + \underbrace{\Delta f_i \phi_{hist}}_{(iia)} + \underbrace{\Delta f_i \phi_{hist,i}^*}_{(iib)} + \underbrace{\Delta f_i \Delta \phi_i}_{(iii)} \right]. \quad (4)$$

Terms (i) and (iii) in Eq. (4) are the same as in Eq. (2b), and the other two terms in the square brackets of Eq. (4) represent (iia) the “effect of the WR frequency change on the climate change signal in precipitation independent of the WR-specific deviation from the climatology” and (iib) the “effect of the WR frequency change on the climate change signal in precipitation due to the WR-specific deviation from the climatology”.

There are two benefits of this additional decomposition: firstly, the term (iib) can take either sign irrespective of the sign of Δf_i , which makes this term more easily interpretable than term (ii). For instance, if a particularly dry weather regime ($\phi_{hist,i}^* < 0$) becomes more frequent ($\Delta f_i > 0$), then term (iib) is negative, while term (ii) is always positive for a

positive Δf_i . Secondly, the term (iia), i.e., $\Delta f_i \phi_{\text{hist}}$, which can be significantly larger than the other terms, cancels to zero when summed over all WRs (because $\sum_{i=1}^n \Delta f_i = 0$). Making the assumption that the residual (term iii) is small (to be verified a posteriori), Eq. (4) can be reduced to

$$\phi_{\text{eoc}} - \phi_{\text{hist}} \approx \sum_{i=1}^n \left[\underbrace{f_{\text{hist},i} \Delta \phi_i}_{(i)} + \underbrace{\Delta f_i \phi_{\text{hist},i}^*}_{(iib)} \right]. \quad (5)$$

The objective of this paper can now be formulated mathematically. It is to investigate the contribution of the frequency change term (iib) compared to the intensity change term (i), for each WR i . The modulus of this ratio is denoted as $\gamma_i(\phi)$ and given by

$$\gamma_i(\phi) := \left| \frac{\frac{\Delta f_i}{f_{\text{hist},i}}}{\frac{\Delta \phi_i}{\phi_{\text{hist},i}^*}} \right|. \quad (6)$$

We consider the modulus of this ratio as we are interested in how the magnitudes of frequency and intensity changes compare, while the sign of the ratio would indicate whether frequency and intensity changes share the same sign or oppose one another.

Note that $\gamma_i(\phi)$ is a field and can be calculated at every model grid point. The question of whether frequency changes of WR i are important for explaining climate change signals in ϕ can now be posed more precisely as, “how large are the fields $\gamma_i(\phi)$?”, where $i = 1, \dots, n$. A large $\gamma_i(\phi)$ indicates a greater importance of frequency changes of WR i for explaining climate change signals in ϕ than a small $\gamma_i(\phi)$. Interestingly, $\gamma_i(\phi)$ depends on three independent factors (see Eq. 6):

1. $\frac{\Delta f_i}{f_{\text{hist},i}}$, which is the relative frequency change of WR i due to climate change. Since climate change does not completely alter the large-scale circulation, it is reasonable to assume that this factor has values on the order of 0.1; i.e., if a certain WR occurs with a frequency of 10 % in the historical climate, it will occur with a frequency in the range of 9 %–11 % in the end-of-century climate. γ_i is directly proportional to this factor.
2. $\Delta \phi_i$, which is the climate change effect on the intensity of the parameter ϕ in the WR i . It corresponds to the average value of ϕ on days in WR i in the end-of-century climate, $\phi_{\text{eoc},i}$, minus the same average in the historical climate, $\phi_{\text{hist},i}$. γ_i is inversely proportional to this factor, and therefore γ_i becomes larger when this factor is small, i.e., if climate change does not affect the WR-specific intensity of parameter ϕ . It is difficult to estimate the magnitude of this factor a priori. The expression for γ_i tells us that we should compare the magnitude of this term with $\phi_{\text{hist},i}^*$. Both this and the previous factor depend on the magnitude of climate change.

3. $\phi_{\text{hist},i}^*$, which is the WR-specific anomaly of parameter ϕ . This factor does not depend on climate change; it is rather a measure for the ability (or skill) of the WR classification in separating contrasting situations in terms of the parameter ϕ . Two idealized cases shed further light on the role of this factor: if each day within the historical period was randomly attributed to a WR, then the average of ϕ would be the same for all WRs and therefore $\phi_{\text{hist},i}^* = 0$ for all WRs (i). In this case $\gamma_i = 0$; i.e., WR frequency changes are completely irrelevant because the WRs do not distinguish different scenarios of ϕ . The opposite case is a highly skillful WR classification, which separates days with strongly positive anomalies of ϕ from those with strongly negative anomalies of ϕ . In this situation the magnitude of $\phi_{\text{hist},i}^*$ can be large, i.e., comparable to the day-to-day variance of ϕ . Now, what matters for γ_i is the ratio of factors (2) and (3), $\frac{\Delta \phi_i}{\phi_{\text{hist},i}^*}$. Note that this is not the ratio $\frac{\Delta \phi_i}{\phi_{\text{hist},i}}$, i.e., the relative intensity change of ϕ in WR i , which would be much smaller. Rather it is the ratio of intensity change to the WR-specific *anomaly* of ϕ . For a “very good WR classification” in terms of the variable ϕ , $\phi_{\text{hist},i}^*$ might be 10 times larger than $\Delta \phi_i$, and in this case we would obtain $\gamma_i = 1$ (for the above-mentioned assumption that $\frac{\Delta f_i}{f_{\text{hist},i}}$ is on the order of 0.1); i.e., in this case the frequency change of WR i would be as important as the intensity change of WR i . As an aside, we note that different measures were previously used for assessing the quality of a WR classification for a given parameter ϕ , e.g., the Brier skill score (Schiemann and Frei, 2010) or the “coefficient of efficiency” (Madonna et al., 2021).

In summary, $\gamma_i(\phi)$ depends on the climate change effect on the frequency of the WR and on the WR-specific intensity change of ϕ , as well as on the skill of the WR classification to separate different states of ϕ . As we will see in the remainder of this paper, it appears difficult to obtain values of $\gamma_i(\phi)$ that are $O(1)$. This is the case at least for the parameter we investigate (surface precipitation, $\phi = P$), for the climate simulations we use (CESM1-LE for the RCP8.5 scenario), and for our WR classification in the North Atlantic–European region. We also show that $\gamma_i(P)$ varies spatially, mainly because of spatial variations of the third factor, i.e., the ability of the WR classification to represent local variability in the considered parameter ϕ . Of course, we do not exclude the possibility that other WR classifications in other regions applied to other parameters could lead to larger values of $\gamma_i(\phi)$ than the ones documented in this study. This would require a combination of a more skillful classification, larger frequency changes, and smaller intensity changes.

In order to test the sampling sensitivity of the decomposition of $\Delta \phi$ into WR-specific contributions to the 35 members used in each period, we implement a bootstrap procedure. For a given season and parameter ϕ , we resample ran-

domly with replacement over all members the same numbers of days as in the original data set. We then compute the regime-specific contribution to $\Delta\phi$, the terms in the decomposition of Eq. (5), and the $\gamma_i(\phi)$ parameter in this resampled data set for each WR at each grid point. We repeat this procedure 1000 times in order to give an estimation of the sampling distribution of the different terms. We then compute the probability in this resampled distribution that the value 0 (for the WR-specific contribution to $\Delta\phi$ and the terms in the decomposition of Eq. 5) or 1 (for $\gamma_i(\phi)$) is exceeded or subceeded. This gives a bootstrapped p value for significance at each grid point. We then use a false discovery rate test of 0.1 to take into account spatial correlations (Wilks, 2016), and we flag as significant the grid points that pass this test.

Before we discuss examples of WR-specific $\gamma_i(\phi)$ fields, we note that from Eq. (5) we can also define an overall γ , defined as

$$\gamma_{\text{overall}}(\phi) = \frac{\left| \sum_{i=1}^n \left[\Delta f_i \phi_{\text{hist},i}^* \right] \right|}{\left| \sum_{i=1}^n \left[f_{\text{hist},i} \Delta \phi_i \right] \right|}. \quad (7)$$

We will briefly consider $\gamma_{\text{overall}}(\phi)$ at the end of the paper in Sect. 5 but next focus on the WR-specific $\gamma_i(\phi)$ in Sect. 4.

4 Application to CESM1-LE simulations

In this section, the concept outlined in Sect. 3 is applied to three aspects of precipitation in DJF and JJA (total seasonal precipitation P , number of wet days N_{wet} , and number of heavy-precipitation days N_{heavy}), using the CESM1 climate simulations and the WR identification outlined in Sect. 2. To set the scene, Fig. 2 shows the CESM1 seasonal-mean climatologies in the historical period of precipitation P in DJF and JJA (Fig. 2a and b), of the number of wet days N_{wet} in DJF (Fig. 2e), and of the number of heavy-precipitation days N_{heavy} in DJF (Fig. 2f), together with the corresponding climate change signals of these fields. In DJF, climatological precipitation is largest (within the considered domain) in southwestern Norway (values larger than 10 mm d^{-1}) and reaches beyond 7 mm d^{-1} in local maxima off the US east coast and near South Greenland, Iceland, and Scotland (Fig. 2a). The climate change signal in this season (Fig. 2c) shows negative values in the Labrador Sea, the Irminger Sea, and the Mediterranean, with values of up to -2 mm d^{-1} , and, in most of the rest of the domain, slightly weaker positive values with local maxima over the UK and southwestern Norway. In JJA, precipitation is weaker in most parts of the North Atlantic compared to DJF (Fig. 2b), and the climate change signals are positive along the North American east coast and in Greenland and negative over most parts of Europe (Fig. 2d). Considering again DJF, the climatological wet-day frequency has high values (0.6–0.9) in large parts of the North Atlantic (Fig. 2e), and climate change signals are positive in the Arctic and over the

Baltic Sea and negative in the same regions as where mean precipitation also decreases (Fig. 2g). Finally, the DJF climatology of N_{heavy} shows a constant value of 0.01 by definition (Fig. 2f), with the largest increases due to climate change in a band along 50° N from Newfoundland to eastern Europe (Fig. 2h).

To explain the steps required for the calculation of γ_i , we now first, in Sect. 4.1, assess as an illustrative example the contributions of the frequency and intensity changes of one selected WR to the climate change signal of P in DJF. Then, in Sect. 4.2 and 4.3, results are shown for different WRs in DJF and JJA and for the three considered aspects of precipitation.

4.1 An illustrative example

As a first example, we consider the frequency and intensity contributions from regime AT (Atlantic Trough) to the climate change signal in P in DJF (Fig. 2c). We have chosen this WR because, in our simulations, it has one of the largest frequency changes in DJF between the two climate periods, from $f_{\text{hist,AT}} = 13.8\%$ to $f_{\text{eoc,AT}} = 15.1\%$ (Fig. 1). For this WR, the relative frequency change of $\frac{\Delta f_{\text{AT}}}{f_{\text{hist,AT}}} = 9.4\%$ corresponds to the first factor relevant to the calculation of γ_i (see Eq. 6). Also, this WR is interesting as it has a strongly positive climate change signal over the British Isles and in the North Sea region (Fig. 3a), i.e., in a region where CMIP6 models show an increase in cyclone track density in DJF (Priestley and Catto, 2022, their Fig. 2e).

According to Eq. (5), the total contribution of regime AT to the climate change signal of P in DJF, i.e., $f_{\text{eoc,AT}} P_{\text{eoc,AT}} - f_{\text{hist,AT}} P_{\text{hist,AT}}$ (Fig. 3a), can be decomposed into a contribution from intensity changes during regime AT (term i, Fig. 3b) and frequency changes of regime AT (term iib, Fig. 3c). As explained in Sect. 3, we use a bootstrap procedure to test the sensitivity of this decomposition to the sampling uncertainty using 35 members and color in white grid points where the change is not significantly different from 0, i.e., when there is no significant change between the two periods. Overall, intensity changes (Fig. 3b) clearly determine the pattern shown in Fig. 3a, including the regions with pronounced positive and negative climate change effects on P . An exception is the region near the Bay of Biscay, where term (iib) has large positive values exceeding 0.1 mm d^{-1} (Fig. 3c), comparable to those from term (i). The reason for this strong local signal is that the WR-specific precipitation anomaly, $P_{\text{hist,AT}}^*$, has large positive values in this region; i.e., precipitation is strongly enhanced in this region in regime AT compared to the climatology. Peak values of $P_{\text{hist,AT}}^*$ in the Bay of Biscay exceed 4 mm d^{-1} (contours in Fig. 3c). Together with the AT frequency change of 1.3 %, this yields the comparatively large values of term (iib). The high values of $P_{\text{hist,AT}}^*$ qualitatively agree with the increased frequency of intense precipitation related to atmo-

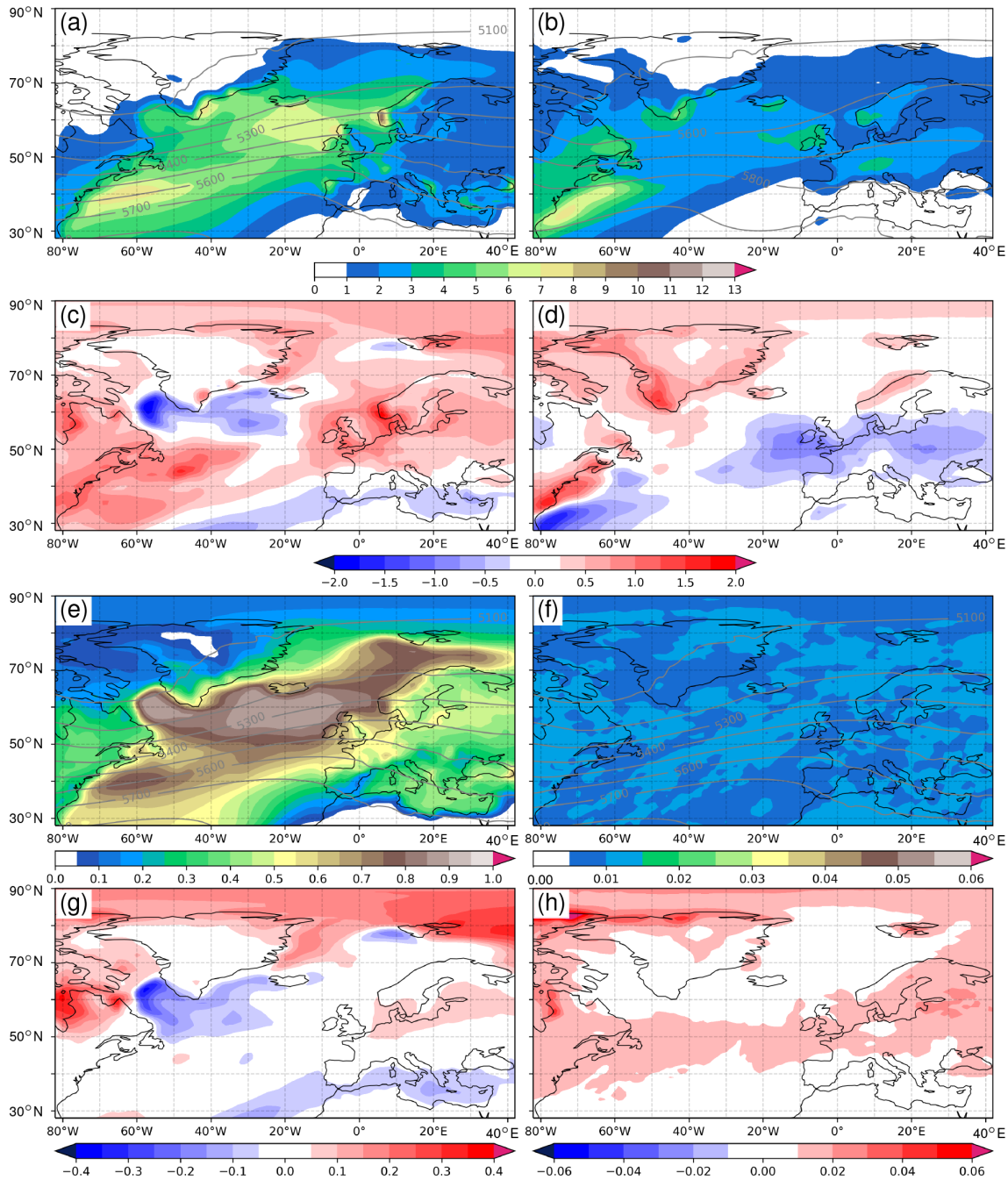


Figure 2. Seasonal-mean precipitation P_{hist} in the CESM1 historical simulations for (a) DJF and (b) JJA and (c, d) the climate change signal $\Delta P = P_{\text{eoc}} - P_{\text{hist}}$ in the same seasons. Units are mm d^{-1} . Seasonal-mean frequency of (e) wet days N_{wet} and (f) heavy-precipitation days N_{heavy} for DJF and (g, h) the climate change signal $\Delta N_{(\cdot)} = N_{(\cdot),\text{eoc}} - N_{(\cdot),\text{hist}}$ in the same season. Values for N_{wet} and N_{heavy} range from 0 to 1. Gray contours in (a), (b), (e), and (f) denote seasonal-mean geopotential height at 500 hPa (in m).

spheric rivers in this region and WR, as shown by Pasquier et al. (2019).

As a consequence, the key field $\gamma_i(\phi)$ investigated in this study, which corresponds to the modulus of the ratio of the fields shown in Fig. 3c (term iib in Eq. 5) and Fig. 3b (term i in Eq. 5), attains for this particular example applica-

tion (total precipitation P , season DJF, regime AT) mainly low values of about $\gamma_{\text{AT}}(P) < 0.125$, except for in the Bay of Biscay region, where $\gamma_{\text{AT}}(P) > 1$ (Fig. 3d). In this panel (Fig. 3d), we use the bootstrap procedure to test whether the absolute value of one term in the decomposition of Eq. (5) is significantly larger than the other one, i.e., whether $\gamma_i(\phi)$

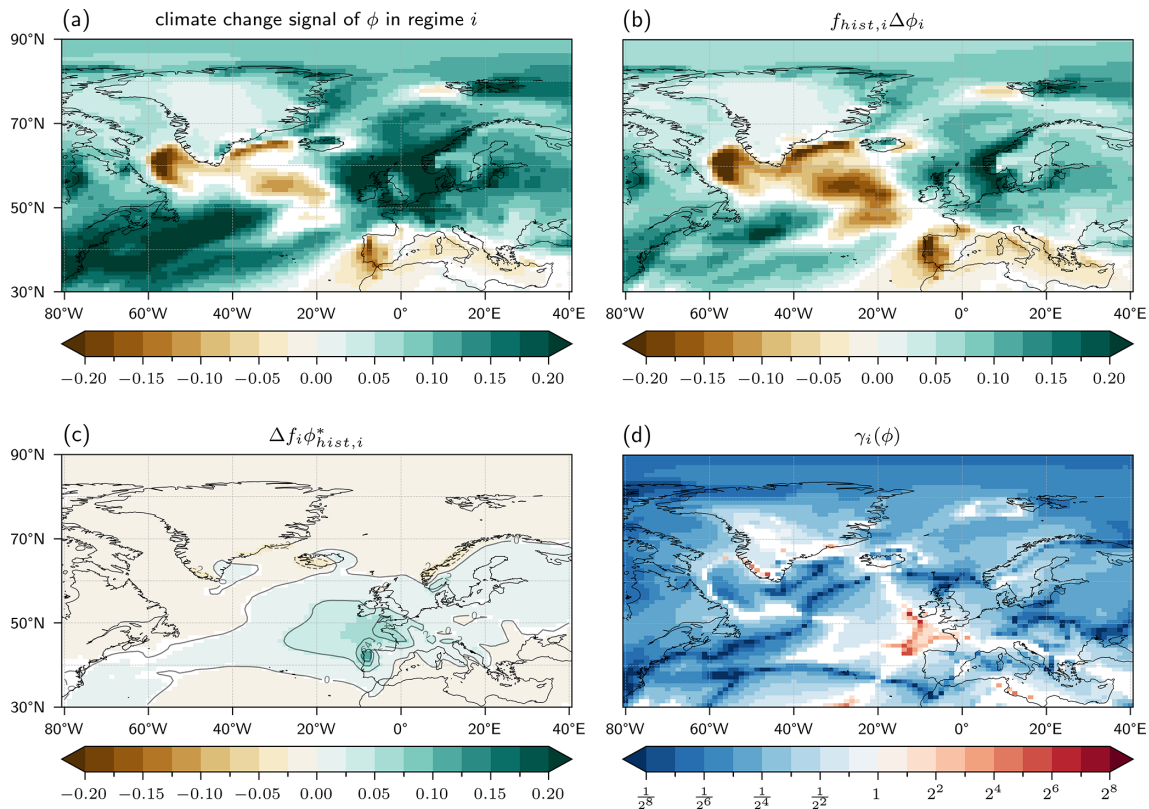


Figure 3. (a) Contribution of the regime AT to the climate change signal of seasonal-mean precipitation $\phi = P$ in DJF (in mm d^{-1}), i.e., $f_{\text{eoc,AT}} P_{\text{eoc,AT}} - f_{\text{hist,AT}} P_{\text{hist,AT}}$; (b) contribution to the field shown in (a) from intensity changes of P in the regime AT, i.e., term (i) in Eq. (5), $f_{\text{hist,AT}} \Delta P_{\text{AT}}$ (in mm d^{-1}); (c) contribution to the field shown in (a) from frequency changes of regime AT, i.e., term (iib) in Eq. (5), $\Delta f_{\text{AT}} P_{\text{hist,AT}}^*$ (in mm d^{-1}); and (d) $\gamma_{\text{AT}}(P)$ in dimensionless units. Contour lines in (c) are $P_{\text{hist,AT}}^*$ (in mm d^{-1}). In (a)–(c), white grid points indicate that the field is not significantly different from 0, i.e., that there is no significant change between the two periods. In (d), white grid points indicate that the values of $\gamma_{\text{AT}}(P)$ are not significantly different from 1, i.e., that the two terms in Eq. (5) are comparable.

is significantly different from 1. Grid points are colored in white when the intensity of the two terms are comparable. Note that this metric should be read in addition to the ones from Fig. 2b and c: a large or small value of $\gamma_i(\phi)$ means that one term largely dominates the other, but a value close to 1 may mean that the two are compensating each other (equal intensity but opposite sign) or that they are of the same order of magnitude (equal intensity and same sign). In some regions the effects of intensity and frequency changes have the opposite sign. For instance, over northwestern Spain, precipitation intensity in regime AT decreases due to climate change (Fig. 3b), whereas the frequency increase of AT contributes to an increase in P (Fig. 3c) – because of a strongly positive AT-specific precipitation anomaly – resulting in a small negative net decrease in winter precipitation associated with regime AT (Fig. 3a). This first example indicates that most of the climate change signal of P in DJF that can be attributed to regime AT is determined by the field of precipitation intensity change associated with the regime and is not due to a frequency change of the regime. However, locally, frequency changes can matter (as shown by values of $\gamma_{\text{AT}}(P)$

on the order of 1 or larger) if they are comparably large and if the considered regime has a locally pronounced precipitation anomaly $P_{\text{hist},i}^*$.

4.2 Systematic analysis of γ_i for total precipitation in DJF and JJA

The same procedure, outlined above for the regime AT, can now be applied to all WRs in DJF in order to obtain the full decomposition of the climate change signal of P into WR-specific intensity and frequency changes. Figure 4 shows the results for the regimes AR, EuBL, ZO, and, for comparison, again AT. The patterns of the total WR contribution to the climate change signal (left column) show many similarities (e.g., negative values in the Labrador Sea and in most of the Mediterranean and positive values over the eastern US and the region extending from the UK to the Baltic Sea). Indeed, these regime-specific climate change signals in P look at first sight very similar to the overall climate change signal in P (Fig. 2c). This means that the climate change signal is, at least in some regions, mainly determined by factors

other than the circulation variability captured by the weather regimes. A prominent example is the strong decrease in precipitation in the Labrador Sea in all regimes. This is caused by the poleward retreat of the sea ice edge in the future climate, which will strongly reduce shallow convection associated with intense cold-air outbreaks south of the sea ice edge in the current climate. However, closer inspection of the left column panels in Fig. 4 also shows important differences between the regimes: (i) south of Iceland, the climate change signal is either strongly negative, strongly positive, or close to zero in the regimes AT, AR, and EuBL and (ii) also in the Iberian Peninsula and along the west coast of Scandinavia there are large differences between the regimes.

As discussed for regime AT in the previous section, these regime-specific climate change signals are mainly, or even almost entirely, due to WR-specific intensity changes (second column in Fig. 4). The role of frequency changes of WRs, which was discussed to be locally important for regime AT, is smaller for all other regimes (third column). For regime ZO, the term (iib) in Eq. 5 is not significantly different from zero (because of the small value of $\Delta f_{ZO} = -0.2$), and therefore, Fig. 4o is all white. Consequently, in this regime, as well as for the regimes that are not shown, the values of $\gamma_i(P)$ hardly exceed 0.1 (right column), indicating that intensity changes are at least 10 times more important than frequency changes for explaining climate change signals of P in these regimes. For AR, $\gamma_{AR}(P)$ reaches values above 0.5 southwest of Iceland.

The same analysis for JJA (Fig. 5) shows first of all generally smaller climate change signals compared to DJF (compare panels in left columns). In regions where there is still a substantial climate change signal, i.e., in regions that are not masked in the plots of $\gamma_i(P)$, the analysis reveals mainly low values of $\gamma_i(P)$ (in most regions smaller than 0.25). The exception is the high values of $\gamma_{AR}(P) > 2$ in a band stretching from west of Ireland to Denmark. These values result from the exceptionally large relative frequency increase of almost 25 % (Fig. 1) and a pronounced dry WR-specific anomaly of P in this region (of about -1.5 mm d^{-1} ; see contours in Fig. 5g). For EuBL, the smaller relative frequency change and similar WR-specific precipitation anomalies lead to values of $\gamma_i(P) \simeq 1$. Except for these two regimes, WR-specific precipitation anomalies of P over Europe tend to be lower in JJA than in DJF (compare contours in the third column of Figs. 4 and 5), indicating that P in JJA, compared to DJF, differs less between WRs. This translates directly into low values of the frequency change terms (iib) and therefore into low values of $\gamma_i(P)$ in most regimes in JJA.

4.3 Systematic analysis of γ_i for the frequency of wet days and heavy-precipitation days in DJF

We now return to the season DJF but consider two different aspects of precipitation climatology: the decomposition is now applied to the number of wet days N_{wet} and to the

number of heavy-precipitation days N_{heavy} (as defined in Sect. 2.1). Figure 6 shows the results for N_{wet} , for the same four WRs as shown previously for P . First, we note that the climate change signals of N_{wet} (left column) are qualitatively similar to those for P , i.e., seasonal-mean wetting in a particular WR typically goes along with more wet days in the same WR, and vice versa for drying. The exception here is the western North Atlantic, where the climate change signal of N_{wet} is close to zero, despite a strong increase in P . And as with P , also for N_{wet} a large part of the climate change signal is explained by the “intensity changes” (second column in Fig. 6). This means that, for instance, the reduction of the contribution from regime AT to the number of wet days in the Mediterranean (Fig. 6a) is mainly due to a reduced rate of wet-day occurrence in regime AT in this region. Consequently, values of $\gamma_{AT}(N_{\text{wet}})$ again tend to be small (less than 0.25) in most regions. Considering all WRs shown in Fig. 6 and compared with the same analysis for P , the $\gamma_i(N_{\text{wet}})$ values appear to be slightly larger.

In stark contrast, for the number of heavy-precipitation days shown in Fig. 7, the climate change signals are positive in almost the entire North Atlantic–European region, but the gamma values are small for all WRs and hardly exceed values of 0.125. This shows that for the frequency of heavy-precipitation days, i.e., for a characteristic of the precipitation climatology that is strongly determined by thermodynamics, WR frequency changes play an even smaller role than they do for, e.g., the frequency of wet days.

5 Conclusions

In this study, we introduced a framework that helps quantify the role of changes in the frequency of WRs in climate change signals in surface precipitation. This framework is conceptually simple and can be applied to any meteorological variable, WR definition, and climate change signal from any climate model and climate change scenario. As a key variable, we suggest calculating the parameter $\gamma_i(\phi)$, which corresponds, for a specific WR i , to the ratio of the contribution from WR frequency changes to the climate change signal of ϕ to the contribution of WR intensity changes. A value of 1 indicates that both contributions are equally important, although this may be because the two terms have either equal intensity and the opposite sign (compensation effect) or equal intensity and same sign (intensification effect). The derivation of $\gamma_i(\phi)$ shows that, for a given WR i , it depends on three independent factors: (i) the relative frequency change of the WR i due to climate change, (ii) the climate change effect on the intensity of the parameter ϕ in the WR i , and (iii) the anomaly of ϕ in WR i , which depends on the skill of the WR classification to separate contrasting situations in terms of the parameter ϕ .

When applying this framework to seasonal-mean precipitation in the North Atlantic–European region in DJF and

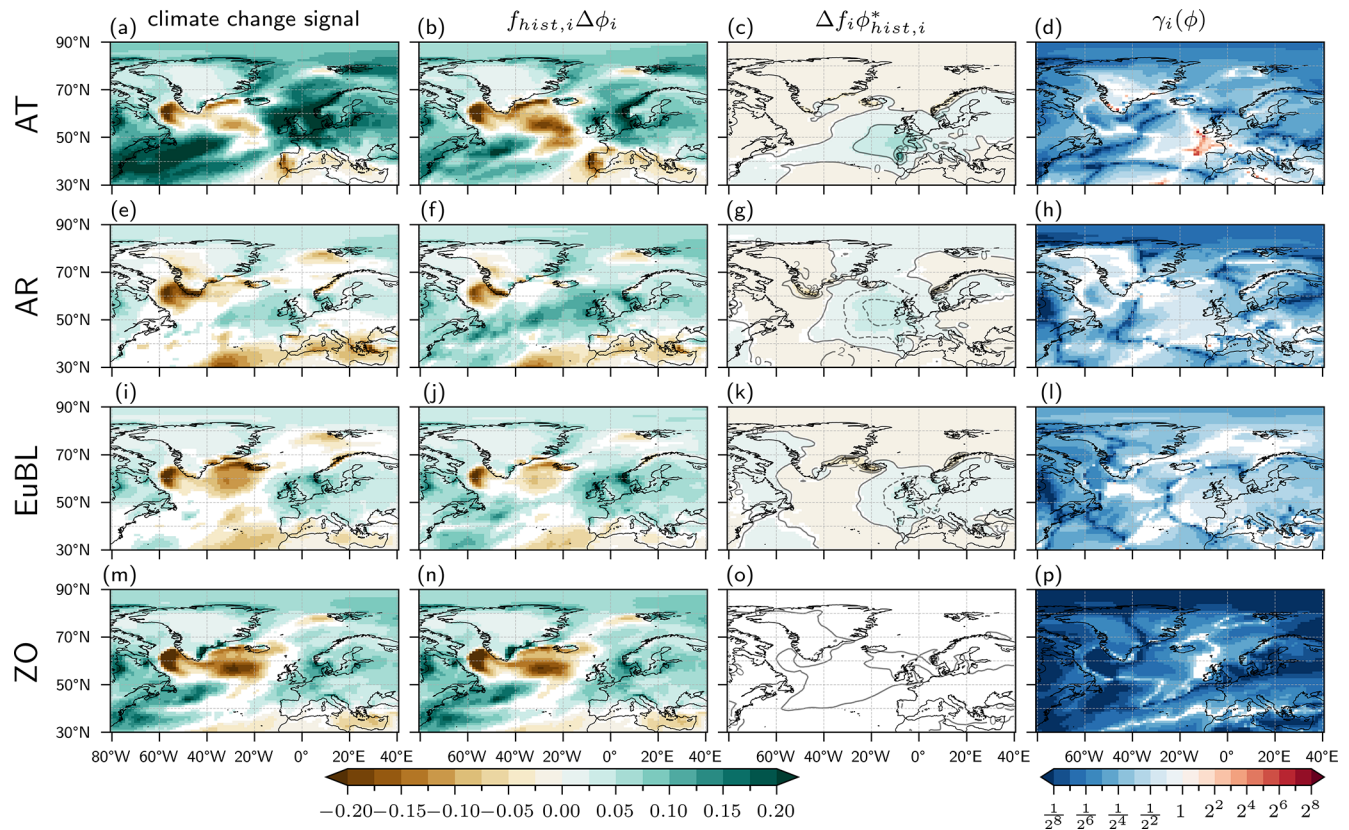


Figure 4. Decomposition of climate change signal of seasonal-mean precipitation P in DJF for regimes (from top to bottom) AT, AR, EuBL, and ZO. **(a, e, i, m)** Total contributions of the regimes to the climate change signal (in mm d^{-1}); **(b, f, j, n)** contributions from WR-specific intensity changes, i.e., term (i) in Eq. (5); **(c, g, k, o)** contributions from WR-specific frequency changes, i.e., term (iib) in Eq. (5); **(d, h, l, p)** $\gamma_i(P)$ in dimensionless units. Contour lines in **(c), (g), (k), and (o)** are for $\phi_{\text{hist},i}^*$ (in mm d^{-1}), and lines are dashed for negative values.

JJA in CESM1-LE simulations under the RCP8.5 scenario and using a 7-WR classification, it turns out that values of $\gamma_i(P)$ are typically small (< 0.25). Only for few WRs and in comparatively small regions did $\gamma_i(P)$ reach values beyond 1, indicating that in individual WRs the frequency changes can matter in regions where these WRs strongly modulate precipitation occurrence (i.e., where the WR classification is particularly skillful). However, from the field $\gamma_{\text{overall}}(P)$ (Eq. 7; see Fig. 8a), which is less than 0.25 in the entire domain, the main conclusion is that when considering the effects of intensity and frequency changes aggregated across WRs, then indeed, to first order, WR frequency changes are not relevant to explaining climate change signals in P . The same fields for the number of wet and heavy-precipitation days, $\gamma_{\text{overall}}(N_{\text{wet}})$ and $\gamma_{\text{overall}}(N_{\text{heavy}})$, are shown in Fig. 8b and c, and they confirm the results for P . Consistent with the discussion in the previous section, $\gamma_{\text{overall}}(N_{\text{wet}})$ has slightly larger values than $\gamma_{\text{overall}}(P)$ in northern Europe, and the values of $\gamma_{\text{overall}}(N_{\text{heavy}})$ are consistently lower, hardly exceeding 0.05. We would like to mention that during the review process the concern was brought up by one of the reviewers that our values of $\gamma_i(\phi)$ are small because we separately re-

moved the climatological mean from the historical and future ensembles and therefore removed part of the climate change signal on the circulation, thus reducing the amplitude of regime frequency changes. However, since we regard weather regimes as patterns describing the circulation variability relative to the respective climatological mean, we do not see how regime frequency changes between different climates can be calculated in a way that is different from the one we implemented. We trust that future studies can further elaborate on these important conceptual questions.

There is a combination of reasons why, in our analysis, WR frequency changes only play a minor role. Or, to put it differently, there are three ways how, with other climate simulations and/or WR classifications and/or variables ϕ , larger $\gamma_i(\phi)$ values could be obtained. These three ways correspond to the three factors discussed in Sect. 3:

- larger relative frequency changes of WRs – in our case, they are typically less than 10 % and only for regime AR in JJA reach almost 25 %;

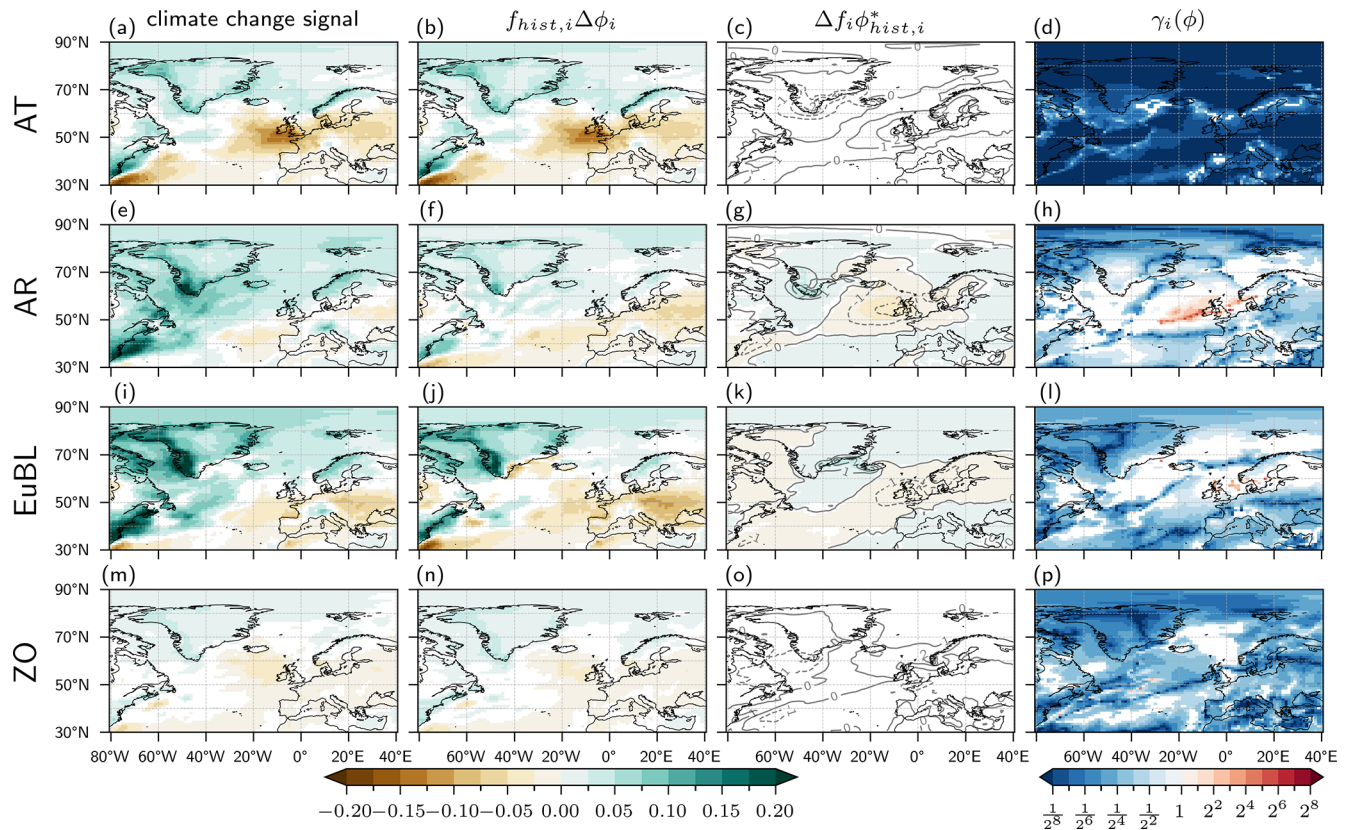


Figure 5. The same as Fig. 4 but for seasonal-mean precipitation P in JJA.

- smaller climate change effects on the intensity of ϕ – these effects are large for $\phi = P$, $\phi = N_{\text{wet}}$, and $\phi = N_{\text{heavy}}$ but might be smaller for other variables; and
- larger WR-specific anomalies of ϕ , i.e., an increased skill of the WR classification in predicting the variable under consideration.

It is worth further discussing the last of these factors. In the rigorous conceptual approach we take here, there is a very explicit dependency of the result, whether WR frequency changes are relevant or not, on the WR classification. Therefore, a comprehensive answer to the question of how important WR frequency changes are for climate change signals should necessarily include a variety of WR classifications. An upper bound to the importance of WR frequency changes would be reached for the “best possible” WR classification, i.e., the WR classification with the largest regime-specific anomalies or the highest skill. A measure for assessing the skill of a WR classification in stratifying precipitation is the Brier skill score (Schiemann and Frei, 2010). It quantifies how much more skillful a WR classification is for predicting daily precipitation, compared to assuming climatological precipitation values. Calculating the Brier skill score for the 60th quantile precipitation threshold and the WR classification used in this study yields values of about 0.2 in western

Europe and lower values in eastern Europe in DJF (Fischer, 2021, their Fig. 4.17). Comparison with the Brier skill scores of more than 70 WR classifications for the 60th quantile of daily precipitation in DJF as reported by Schiemann and Frei (2010), which are between 0.1–0.3, indicates that the skill of our WR classification is within this range. Therefore, it is unlikely that a different WR classification would yield much larger values of $\gamma_i(P)$ in DJF. In JJA, however, the Brier skill score of our Atlantic basin-wide WR classification for the same precipitation quantile is low, with values of less than 0.02 over most of central and eastern Europe.

There are few exceptions to the general result of small values of $\gamma_i(P)$. In some regions in western Europe and for WRs with comparatively large frequency changes, $\gamma_i(P)$ reaches values beyond 1. This geographical preference of larger $\gamma_i(P)$ values in western Europe is related to the fact that precipitation in these regions differs rather strongly between the WRs. In other words, in these regions, the WR classification explains more of the rainfall variability, and therefore, circulation changes as quantified by changing WR frequencies can matter in explaining WR-specific climate change signals in P . As shown in Fig. 8, near the British Isles $\gamma_{\text{overall}}(P)$ reaches its largest values of about 0.25, indicating that in this part of the North Atlantic storm track in DJF, WR frequency changes also contribute about one-fourth

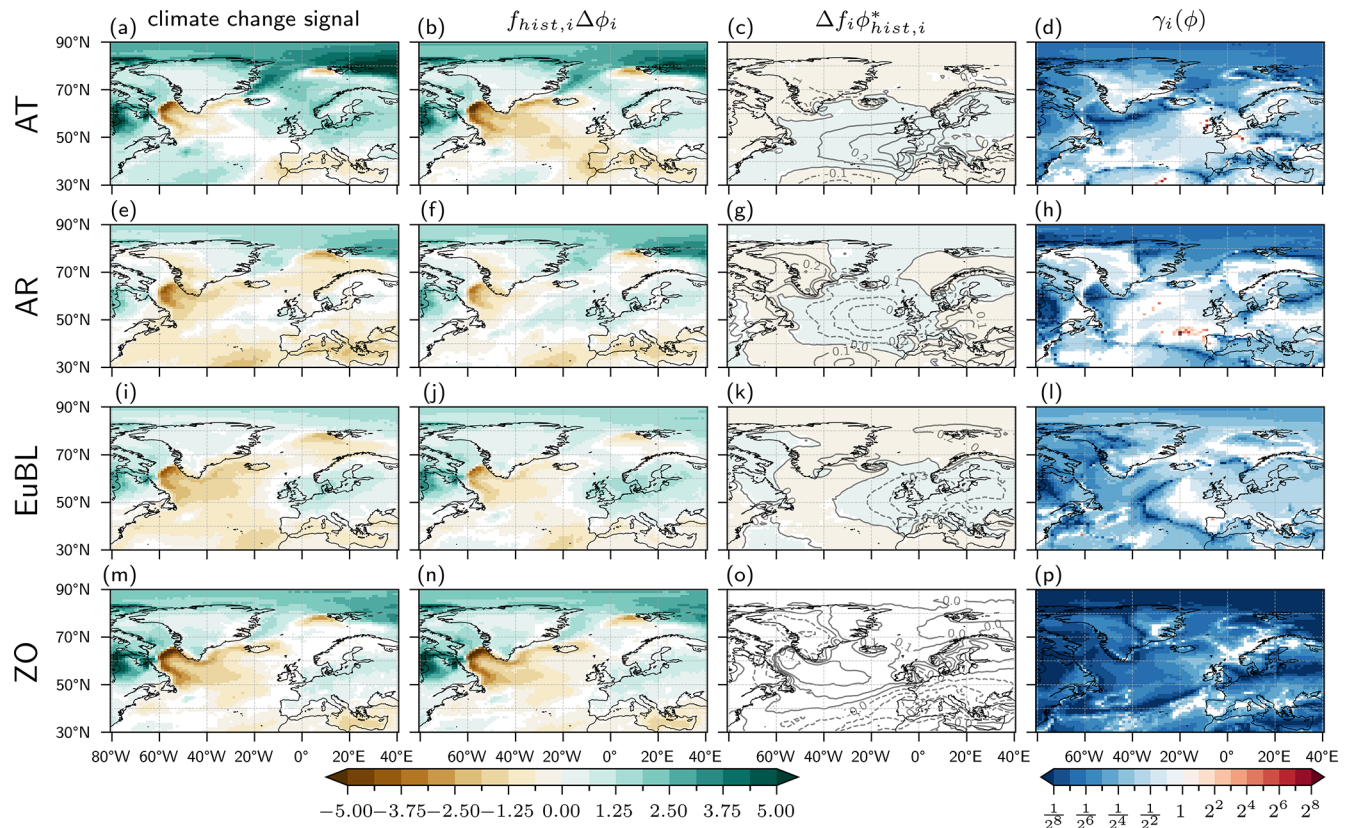


Figure 6. Decomposition of climate change signal for the frequency of wet days N_{wet} in winter (DJF) for regimes as labeled on the left-hand side of each row. Plotting conventions are identical to those in Fig. 4.

to the overall increase in P in the considered climate change simulations (Fig. 2c).

However, the resulting values of $\gamma_i(\phi)$ depend not only on the regime classification, but also clearly on the climate model and the climate change scenario, on the region, and on the parameter ϕ . We hope that the conceptual analysis and examples shown in this study will motivate others to assess $\gamma_i(\phi)$ for different WR classifications, in other regions, and with output from other climate simulations. In terms of different variables, we briefly compared results for three aspects of precipitation and found slightly larger values of $\gamma_i(\phi)$ for the number of wet days N_{wet} than for seasonal-mean precipitation P and the lowest values of $\gamma_i(\phi)$ for the number of heavy-precipitation events N_{heavy} . These differences might be related to the fact that some meteorological variables are affected strongly by climate change through thermodynamic effects, e.g., the intensity of heavy-precipitation events (Pendergrass, 2018) or the frequency of days above a certain absolute temperature threshold. The larger the thermodynamic effect of global warming on a certain variable, the larger (and the more uniform across weather regimes) the intensity change $\Delta\phi_i$ and the smaller the γ_i . Conversely, for variables for which thermodynamic arguments constrain their climate change signal less, no physical reason exists for why $\Delta\phi_i$

should be large (and uniform across weather regimes), and thus we expect larger values of $\gamma_i(\phi)$ for such variables.

Several studies explicitly quantified dynamic vs. thermodynamic contributions to climate change. For instance Pfahl et al. (2017) found that the dynamic contribution to changes in extreme precipitation is mainly important in the subtropics but not in the midlatitudes. This result is qualitatively consistent with our finding that $\gamma_i(N_{\text{heavy}})$ is small in the North Atlantic–European domain. However, it is important to mention that our decomposition into WR frequency and intensity changes cannot be easily compared to this alternative approach of separating thermodynamic and dynamic effects. WR frequency changes can be essentially regarded as dynamic contributions, whereas WR intensity changes most likely have a strong thermodynamic contribution but may also contain a substantial effect from dynamics. For instance, in a warmer climate, intense cyclones may become deeper due to enhanced precipitation and diabatic heating (e.g., Büeler and Pfahl, 2019; Sinclair et al., 2020; Dolores-Tesillos et al., 2022; Binder et al., 2023), and this dynamic contribution would be quantified in our approach as a WR intensity increase (assuming here that the intense cyclones still occur in the same WR). In future studies, it is therefore important to improve the understanding of the WR in-

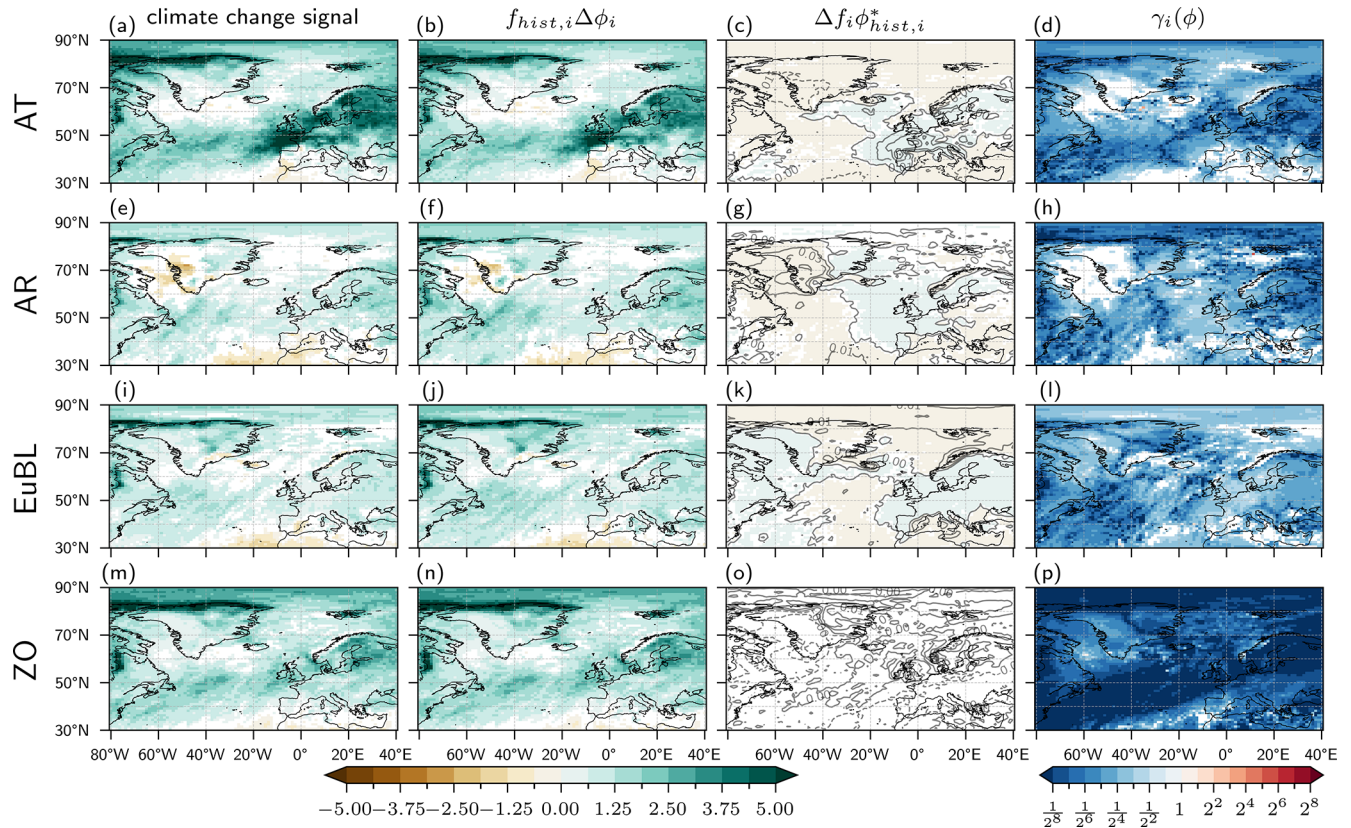


Figure 7. Decomposition of climate change signal for the frequency of heavy-precipitation days N_{heavy} in winter (DJF) for regimes as labeled on the left-hand side of each row. Plotting conventions are identical to those in Fig. 4.

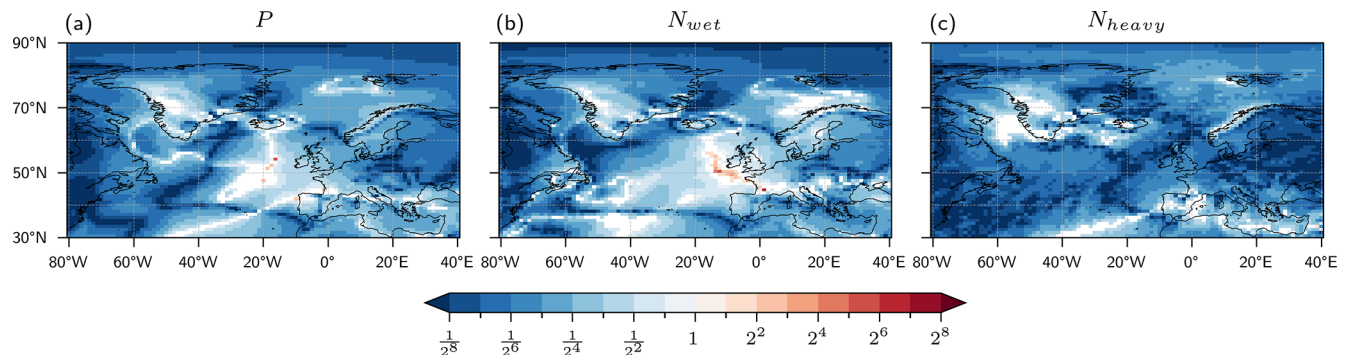


Figure 8. The overall γ_{overall} in DJF as defined in Eq. (7) for (a) seasonal-mean precipitation P , (b) the number of wet days N_{wet} , and (c) the number of heavy-precipitation days N_{heavy} . Plotting conventions are identical to those in the right panels in Fig. 4.

tensity changes. While, at least in some regions, $\Delta\phi_i(P)$ is fairly uniform across WRs (see second column in Fig. 4), which most likely indicates a strong thermodynamic control on these fields, the WR-specific intensity changes for the frequency of heavy-precipitation events, $\Delta\phi_i(N_{\text{heavy}})$ (second column in Fig. 7), are much less uniform, which is likely related to dynamical effects such as the preferred location of intense cyclones in different WRs.

In future studies, the conceptual γ approach could be extended to decompositions based on the frequency of occurrence and intensity of synoptic weather systems such as cyclones, anticyclones, and fronts. That is, instead of asking how WR frequency changes affect climate change signals of, e.g., precipitation, one could diagnose the relevance of frequency changes in the occurrence of cyclones and fronts. Examples of such weather system decomposition were presented in Yettella and Kay (2017) and in Chang et al. (2022).

The approach introduced in this study could provide useful guidance for the analysis and interpretation of how weather system frequencies and intensities affect trends in surface weather parameters.

Code and data availability. For ERA-Interim reanalyses (Dee et al., 2011), the Public Datasets Service closed on 1 June 2023. However, access to the ERA-Interim and CESM-LE fields used in this study is available from the authors upon request. The code of the CESM model (Hurrell et al., 2013) used for the CESM-LE simulations is available from <https://www.cesm.ucar.edu/models/cesm1.0/> (last access: 2 April 2024).

Author contributions. LJF, MR, and HW designed this study, and LJF performed all analyses with support from DB, CMG, and MR. LJF, DB, and HW wrote the manuscript, with feedback about the results and text from all co-authors. RN contributed with the statistical testing and gave feedback on the last version of the paper.

Competing interests. At least one of the (co-)authors is a member of the editorial board of *Weather and Climate Dynamics*. The peer-review process was guided by an independent editor, and the authors also have no other competing interests to declare.

Disclaimer. Publisher's note: Copernicus Publications remains neutral with regard to jurisdictional claims made in the text, published maps, institutional affiliations, or any other geographical representation in this paper. While Copernicus Publications makes every effort to include appropriate place names, the final responsibility lies with the authors.

Acknowledgements. We are very grateful to the thoughtful comments by the two anonymous reviewers and the editor, Camille Li, which helped improve the presentation of our results.

Financial support. Dominik Büeler and Robin Noyelle have received funding from the Schweizerischer Nationalfonds zur Förderung der Wissenschaftlichen Forschung (grant nos. 205419 and 216710, respectively), and Matthias Röthlisberger has received funding from the H2020 European Research Council (INTEXseas, grant no. 787652). The contribution of Christian M. Grams was funded by the Helmholtz Association as part of the Young Investigator Group “Sub-seasonal Predictability: Understanding the Role of Diabatic Outflow” (SPREADOUT, grant VH-NG-1243).

Review statement. This paper was edited by Camille Li and reviewed by two anonymous referees.

References

- Bader, S. and Richner, H.: Grundlagen der Schüepp'schen Alpenwetterstatistik AWS, eine Zusammenstellung der relevanten Dokumente, <https://doi.org/10.3929/ethz-b-000296143>, 2018.
- Barnston, A. G. and Livezey, R. E.: Classification, seasonality and persistence of low-frequency atmospheric circulation patterns, *Mon. Weather Rev.*, 115, 1083–1126, [https://doi.org/10.1175/1520-0493\(1987\)115<1083:CSAPOL>2.0.CO;2](https://doi.org/10.1175/1520-0493(1987)115<1083:CSAPOL>2.0.CO;2), 1987.
- Binder, H., Joos, H., Sprenger, M., and Wernli, H.: Warm conveyor belts in present-day and future climate simulations – Part 2: Role of potential vorticity production for cyclone intensification, *Weather Clim. Dynam.*, 4, 19–37, <https://doi.org/10.5194/wcd-4-19-2023>, 2023.
- Bloomfield, H. C., Brayshaw, D. J., Gonzalez, P. L. M., and Charlton-Perez, A.: Pattern-based conditioning enhances sub-seasonal prediction skill of European national energy variables, *Meteorol. Appl.*, 28, e2018, <https://doi.org/10.1002/met.2018.2021>.
- Büeler, D. and Pfahl, S.: Potential vorticity diagnostics to quantify effects of latent heating in extratropical cyclones. Part II: Application to idealized climate change simulations, *J. Atmos. Sci.*, 76, 1885–1902, <https://doi.org/10.1175/JAS-D-18-0342.1>, 2019.
- Büeler, D., Ferranti, L., Magnusson, L., Quinting, J. F., and Grams, C. M.: Year-round sub-seasonal forecast skill for Atlantic–European weather regimes, *Q. J. Roy. Meteor. Soc.*, 147, 4283–4309, <https://doi.org/10.1002/qj.4178>, 2021.
- Cassano, J. J., Uotila, P., Lynch, A. H., and Cassano, E. N.: Predicted changes in synoptic forcing of net precipitation in large Arctic river basins during the 21st century, *J. Geophys. Res.-Biogeo.*, 112, <https://doi.org/10.1029/2006JG000332>, 2007.
- Cattiaux, J., Douville, H., and Peings, Y.: European temperatures in CMIP5: origins of present-day biases and future uncertainties, *Clim. Dyn.*, 41, 2889–2907, <https://doi.org/10.1007/s00382-013-1731-y>, 2013.
- Chang, E. K.-M., Yau, A. M.-W., and Zhang, R.: Finding storm track activity metrics that are highly correlated with weather impacts. Part II: Estimating precipitation change associated with projected storm track change over Europe, *J. Climate*, 35, 2423–2440, <https://doi.org/10.1175/JCLI-D-21-0259.1>, 2022.
- Coe, D., Barlow, M., Agel, L., Colby, F., Skinner, C., and Qian, J.-H.: Clustering analysis of autumn weather regimes in the northeast United States, *J. Climate*, 34, 7587–7605, <https://doi.org/10.1175/JCLI-D-20-0243.1>, 2021.
- Dee, D. P., Uppala, S. M., Simmons, A. J., Berrisford, P., Poli, P., Kobayashi, S., Andrae, U., Balmaseda, M. A., Balsamo, G., Bauer, P., Bechtold, P., Beljaars, A. C. M., van de Berg, L., Bidlot, J., Bormann, N., Delsol, C., Dragani, R., Fuentes, M., Geer, A. J., Haimberger, L., Healy, S. B., Hersbach, H., Hólm, E. V., Isaksen, I., Kållberg, P., Köhler, M., Matricardi, M., McNally, A. P., Monge-Sanz, B. M., Morcrette, J.-J., Park, B.-K., Peubey, C., de Rosnay, P., Tavolato, C., Thépaut, J.-N., and Vitart, F.: The ERA-Interim reanalysis: configuration and performance of the data assimilation system, *Q. J. Roy. Meteor. Soc.*, 137, 553–597, <https://doi.org/10.1002/qj.828>, 2011.
- Dolores-Tesillos, E., Teubler, F., and Pfahl, S.: Future changes in North Atlantic winter cyclones in CESM-LE – Part 1: Cyclone intensity, potential vorticity anomalies, and hori-

- zontal wind speed, *Weather Clim. Dynam.*, 3, 429–448, <https://doi.org/10.5194/wcd-3-429-2022>, 2022.
- Drücke, J., Borsche, M., James, P., Kaspar, F., Pfeifroth, U., Ahrens, B., and Trentmann, J.: Climatological analysis of solar and wind energy in Germany using the Grosswetterlagen classification, *Renew. Energ.*, 164, 1254–1266, <https://doi.org/10.1016/j.renene.2020.10.102>, 2021.
- Fabiano, F., Meccia, V. L., Davini, P., Ghinassi, P., and Corti, S.: A regime view of future atmospheric circulation changes in northern mid-latitudes, *Weather Clim. Dynam.*, 2, 163–180, <https://doi.org/10.5194/wcd-2-163-2021>, 2021.
- Fischer, L. J.: Assessing the potential to strengthen the resilience of the Swiss hydropower sector based on understanding the role of weather regimes in a changing climate, PhD thesis, ETH Zürich, Switzerland, <https://doi.org/10.3929/ethz-b-000497310>, 2021.
- Gaetani, M., Pohl, B., Alvarez Castro, M. C., Flamant, C., and Formenti, P.: A weather regime characterisation of winter biomass aerosol transport from southern Africa, *Atmos. Chem. Phys.*, 21, 16575–16591, <https://doi.org/10.5194/acp-21-16575-2021>, 2021.
- Grams, C. M., Beerli, R., Pfenninger, S., Staffell, I., and Wernli, H.: Balancing Europe's wind-power output through spatial deployment informed by weather regimes, *Nat. Clim. Change*, 7, 557–562, <https://doi.org/10.1038/nclimate3338>, 2017.
- Hannachi, A., Straus, D. M., Franzke, C. L. E., Corti, S., and Woollings, T.: Low-frequency nonlinearity and regime behavior in the Northern Hemisphere extratropical atmosphere, *Rev. Geophys.*, 55, 199–234, <https://doi.org/10.1002/2015RG000509>, 2017.
- Hess, P. and Brezowsky, H.: Katalog der Grosswetterlagen Europas. Berichte des Deutschen Wetterdienstes in der US-Zone, <https://books.google.ch/books?id=1UfxHwAACAAJ> (last access: 25 September 2025), 1952.
- Hochman, A., Messori, G., Quinting, J. F., Pinto, J. G., and Grams, C. M.: Do Atlantic-European weather regimes physically exist?, *Geophys. Res. Lett.*, 48, 1–10, <https://doi.org/10.1029/2021GL095574>, 2021.
- Horton, D. E., C., J. N., Singh, D., Swain, D. L., Rajaratnam, B., and Diffenbaugh, N. S.: Contribution of changes in atmospheric circulation patterns to extreme temperature trends, *Nature*, 522, 465–469, <https://doi.org/10.1038/nature14550>, 2015.
- Huang, W. T. K., Charlton-Perez, A., Lee, R. W., Neal, R., Saran, C., and Sun, T.: Weather regimes and patterns associated with temperature-related excess mortality in the UK: a pathway to sub-seasonal risk forecasting, *Environ. Res. Lett.*, 15, 124052, <https://doi.org/10.1088/1748-9326/abcbb>, 2020.
- Huguenin, M. F., Fischer, E. M., Kotlarski, S., Scherrer, S. C., Schwierz, C., and Knutti, R.: Lack of change in the projected frequency and persistence of atmospheric circulation types over central Europe, *Geophys. Res. Lett.*, 47, 1–10, <https://doi.org/10.1029/2019GL086132>, 2020.
- Hurrell, J. W., Holland, M. M., Gent, P. R., Ghan, S., Kay, J. E., Kushner, P. J., Lamarque, J.-F., Large, W. G., Lawrence, D., Lindsay, K., Lipscomb, W. H., Long, M. C., Mahowald, N., Marsh, D. R., Neale, R. B., Rasch, P., Vavrus, S., Vertenstein, M., Bader, D., Collins, W. D., Hack, J. J., Kiehl, J., and Marshall, S.: The Community Earth System Model: a framework for collaborative research, *B. Am. Meteorol. Soc.*, 94, 1339–1360, <https://doi.org/10.1175/BAMS-D-12-00121.1>, 2013.
- Jerez, S. and Trigo, R. M.: Time-scale and extent at which large-scale circulation modes determine the wind and solar potential in the Iberian Peninsula, *Environ. Res. Lett.*, 8, 044035, <https://doi.org/10.1088/1748-9326/8/4/044035>, 2013.
- Kay, J. E., Deser, C., Phillips, A., Mai, A., Hannay, C., Strand, G., Arblaster, J. M., Bates, S. C., Danabasoglu, G., Edwards, J., Holland, M., Kushner, P., Lamarque, J.-F., Lawrence, D., Lindsay, K., Middleton, A., Munoz, E., Neale, R., Oleson, K., Polvani, L., and Vertenstein, M.: The Community Earth System Model (CESM) large ensemble project: a community resource for studying climate change in the presence of internal climate variability, *B. Am. Meteorol. Soc.*, 96, 1333–1349, <https://doi.org/10.1175/BAMS-D-13-00255.1>, 2015.
- Lang, A. L., Pegion, K., and Barnes, E. A.: Introduction to special collection: “Bridging weather and climate: subseasonal-to-seasonal (S2S) prediction”, *J. Geophys. Res.-Atmos.*, 125, 1–7, <https://doi.org/10.1029/2019JD031833>, 2020.
- Maddison, J. W., Abalos, M., Barriopedro, D., García-Herrera, R., Garrido-Perez, J. M., and Ordóñez, C.: Linking air stagnation in Europe with the synoptic- to large-scale atmospheric circulation, *Weather Clim. Dynam.*, 2, 675–694, <https://doi.org/10.5194/wcd-2-675-2021>, 2021.
- Madonna, E., Battisti, D. S., Li, C., and White, R. H.: Reconstructing winter climate anomalies in the Euro-Atlantic sector using circulation patterns, *Weather Clim. Dynam.*, 2, 777–794, <https://doi.org/10.5194/wcd-2-777-2021>, 2021.
- Mastrantonas, N., Herrera-Lormendez, P., Magnusson, L., Pappenberger, F., and Matschullat, J.: Extreme precipitation events in the Mediterranean: spatiotemporal characteristics and connection to large-scale atmospheric flow patterns, *Int. J. Climatol.*, 41, 2710–2728, <https://doi.org/10.1002/joc.6985>, 2020.
- Michel, C. and Rivière, G.: The link between Rossby wave breakings and weather regime transitions, *J. Atmos. Sci.*, 68, 1730–1748, <https://doi.org/10.1175/2011JAS3635.1>, 2011.
- Namias, J.: Long range weather forecasting – history, current status and outlook, *B. Am. Meteorol. Soc.*, 49, 438–470, <https://doi.org/10.1175/1520-0477-49.5.438>, 1968.
- Palmer, T. N.: A nonlinear dynamical perspective on climate prediction, *J. Climate*, 12, 575–591, [https://doi.org/10.1175/1520-0442\(1999\)012<0575:ANDPOC>2.0.CO;2](https://doi.org/10.1175/1520-0442(1999)012<0575:ANDPOC>2.0.CO;2), 1999.
- Pasquier, J. T., Pfahl, S., and Grams, C. M.: Modulation of atmospheric river occurrence and associated precipitation extremes in the North Atlantic region by European weather regimes, *Geophys. Res. Lett.*, 46, 1014–1023, <https://doi.org/10.1029/2018GL081194>, 2019.
- Pendergrass, A.: What precipitation is extreme?, *Science*, 360, 1072–1073, <https://doi.org/10.1126/science.aat1871>, 2018.
- Pfahl, S., O’Gorman, P. A., and Fischer, E. M.: Understanding the regional pattern of projected future changes in extreme precipitation, *Nat. Clim. Change*, 7, 423–427, <https://doi.org/10.1038/nclimate3287>, 2017.
- Priestley, M. D. K. and Catto, J. L.: Future changes in the extratropical storm tracks and cyclone intensity, wind speed, and structure, *Weather Clim. Dynam.*, 3, 337–360, <https://doi.org/10.5194/wcd-3-337-2022>, 2022.
- Riediger, U. and Gratzki, A.: Future weather types and their influence on mean and extreme climate indices for precipitation and temperature in central Europe, *Meteorol. Z.*, 23, 231–252, <https://doi.org/10.1127/0941-2948/2014/0519>, 2014.

- Röthlisberger, M., Sprenger, M., Flaounas, E., Beyerle, U., and Wernli, H.: The substructure of extremely hot summers in the Northern Hemisphere, *Weather Clim. Dynam.*, 1, 45–62, <https://doi.org/10.5194/wcd-1-45-2020>, 2020.
- Santos, J. A., Belo-Pereira, M., Fraga, H., and Pinto, J. G.: Understanding climate change projections for precipitation over western Europe with a weather typing approach, *J. Geophys. Res.-Atmos.*, 121, 1170–1189, <https://doi.org/10.1002/2015JD024399>, 2016.
- Schiemann, R. and Frei, C.: How to quantify the resolution of surface climate by circulation types: An example for Alpine precipitation, *Phys. Chem. Earth*, 35, 403–410, <https://doi.org/10.1016/j.pce.2009.09.005>, 2010.
- Schüepp, M.: Die Klassifikation der Witterungslagen, *Pure Appl. Geophys.*, 44, 242–248, <https://doi.org/10.1007/BF01997652>, 1959.
- Sinclair, V. A., Rantanen, M., Haapanala, P., Räisänen, J., and Järvinen, H.: The characteristics and structure of extra-tropical cyclones in a warmer climate, *Weather Clim. Dynam.*, 1, 1–25, <https://doi.org/10.5194/wcd-1-1-2020>, 2020.
- Tveito, O. E. and Huth, R.: Circulation-type classifications in Europe: results of the COST 733 Action, *Int. J. Climatol.*, 36, 2671–2672, <https://doi.org/10.1002/joc.4768>, 2016.
- van der Wiel, K., Bloomfield, H. C., Lee, R. W., Stoop, L. P., Blackport, R., Screen, J. A., and Selten, F. M.: The influence of weather regimes on European renewable energy production and demand, *Environ. Res. Lett.*, 14, 094010, <https://doi.org/10.1088/1748-9326/ab38d3>, 2019.
- Vautard, R.: Multiple weather regimes over the North Atlantic: analysis of precursors and successors, *Mon. Weather Rev.*, 118, 2056–2081, [https://doi.org/10.1175/1520-0493\(1990\)118<2056:MWROTN>2.0.CO;2](https://doi.org/10.1175/1520-0493(1990)118<2056:MWROTN>2.0.CO;2), 1990.
- Vigaud, N., Robertson, A. W., and Tippett, M. K.: Predictability of recurrent weather regimes over North America during winter from submonthly reforecasts, *Mon. Weather Rev.*, 146, 2559–2577, <https://doi.org/10.1175/MWR-D-18-0058.1>, 2018.
- Wilks, D.: “The stippling shows statistically significant grid points”: how research results are routinely overstated and overinterpreted, and what to do about it, *B. Am. Meteorol. Soc.*, 97, 2263–2273, <https://doi.org/10.1175/BAMS-D-15-00267.1>, 2016.
- Yettella, V. and Kay, J. E.: How will precipitation change in extratropical cyclones as the planet warms? Insights from a large initial condition climate model ensemble, *Clim. Dynam.*, 49, 1765–1781, <https://doi.org/10.1007/s00382-016-3410-2>, 2017.
- Yiou, P. and Nogaj, M.: Extreme climatic events and weather regimes over the North Atlantic: when and where?, *Geophys. Res. Lett.*, 31, L07202, <https://doi.org/10.1029/2003GL019119>, 2004.
- Yiou, P., Servonnat, J., Yoshimori, M., Swingedouw, D., Khodri, M., and Abe-Ouchi, A.: Stability of weather regimes during the last millennium from climate simulations, *Geophys. Res. Lett.*, 39, L08703, <https://doi.org/10.1029/2012GL051310>, 2012.
- Zappa, G., Hawcroft, M. K., Shaffrey, L., Black, E., and Brayshaw, D. J.: Extratropical cyclones and the projected decline of winter Mediterranean precipitation in the CMIP5 models, *Clim. Dynam.*, 45, 1727–1738, <https://doi.org/10.1007/s00382-014-2426-8>, 2015.
- Zhang, Z. and Wang, K.: The synoptic to decadal variability in the winter surface wind speed over China by the weather regime view, *Geophys. Res. Lett.*, 48, e2020GL091994, <https://doi.org/10.1029/2020GL091994>, 2021.